IOP Publishing Measurement Science and Technology
Meas. Sci. Technol. **30** (2019) 025201 (9pp) https://doi.org/10.1088/1361-6501/aaf4d0

Calibration of polarization effect of a high-numerical-aperture objective lens with Mueller matrix polarimetry

Chao Chen[1], Xiuguo Chen[1], Honggang Gu[1], Hao Jiang[1], Chuanwei Zhang[1,2] and Shiyuan Liu[1,2]

[1] State Key Laboratory for Digital Manufacturing Equipment and Technology, Huazhong University of Science and Technology, Wuhan 430074, People's Republic of China
[2] Wuhan Eoptics Technology Co. Ltd., Wuhan 430075, People's Republic of China

E-mail: xiuguochen@hust.edu.cn and shyliu@hust.edu.cn

Received 23 July 2018, revised 21 November 2018
Accepted for publication 29 November 2018
Published 21 December 2018

Abstract

The calibration of the polarization effect of a high-numerical-aperture (high-NA) objective lens (OL) is of great significance for high-precision polarized light micro-imaging. In this work, we propose a method to calibrate the polarization effect of a high-NA OL with Mueller matrix polarimetry in a retro-reflection configuration by using a spherical mirror as the reference sample. We present the calibration details in both the conoscopic and orthoscopic illumination modes. A high-NA OL with a NA of 0.95 is exemplified to demonstrate the capability of the proposed calibration method, and the experiments performed on two standard SiO_2/Si thin film samples with thicknesses of 25 nm and 100 nm verify the calibrated results. Compared with the existing calibration methods, the proposed method is simpler and more efficient for implementation, and moreover, the calibrated Mueller matrices contain all the polarization information of the high-NA OL under test. It is therefore expected that the proposed calibration method could provide a more complete polarization characterization of the high-NA OL.

Keywords: polarized light imaging, polarization effect, numerical aperture, objective lens, Mueller matrix, polarimetry, Mueller matrix decomposition

(Some figures may appear in colour only in the online journal)

1. Introduction

Polarized light micro-imaging that combines optical microscopy with polarization modulation techniques plays an important role in various research fields, such as optical mineralogy [1], optical crystallography [2], biomedicine [3–5], and metrology [6–9]. To acquire more details of spatially distributed information of a sample, a high-numerical-aperture (high-NA) objective lens (OL) is often employed for a high lateral resolution. On the other hand, by introducing a high-NA OL, the assumption that the transmitted wavefront has uniform amplitude and constant polarization state across the exit pupil cannot be valid any more in most polarized light micro-imaging systems. It is because a high-NA OL is a complicated system with intricate combination of lenses and films bringing non-negligible amplitude variations and wavefront differences between the two polarization components [10, 11]. The intrinsic polarization effect of a high-NA OL has become one of the most important factors affecting the performance of a polarized light micro-imaging system [12]. The calibration of the polarization effect of a high-NA OL is thus of great significance for high-precision polarization imaging.

The calibration of polarization effect of a high-NA OL involves at least two issues. The first one is the characterization of the polarization effect, and the second one is then the measurement of the characterized polarization effect. Several approaches have been proposed to characterize the polarization effect of a high-NA OL, such as the Jones matrix, the

Pauli spin matrix, and the Mueller matrix [12, 13]. Among these approaches, the Mueller matrix representation will be adopted in this paper based on the following considerations. First, compared with other approaches, the Mueller matrix provides much more abundant polarization information, such as retardance, diattenuation, and depolarization. Actually, the 16 elements of a 4×4 Mueller matrix contain all the polarization information that one can extract from a linear polarization scattering process. Second, the Mueller matrix can be directly measured by a Mueller matrix polarimeter (MMP) [14], which is also known as a Mueller matrix ellipsometer (MME) in the characterization of refractive indices and thicknesses of thin films and geometrical profiles of nanostructures [15].

Most of the references in the literature about the calibration of polarization effect of a high-NA OL are found in optical lithography for the calibration of the projection lens [16–20]. In the calibration of the lithographic projection lens with MMP, the MMP measurements are typically carried out in a straight-through configuration [19, 20]. In addition to an extra collimator lens required in the straight-through configuration, the MMP also needs equipping with specially designed polarimeter masks composed of thin-plate polarizers and wide-view-angle quarter-wave plates, which makes the calibration setup complicated. A simpler setup was reported in [21], where the MMP measurements were performed in a retro-reflection configuration by using a spherical mirror (SM) as the reference sample. In the calibration, the center of the SM was aligned to make it in coincidence with the front focal point of the OL under test. In this case, the Mueller matrix of the SM is always a diagonal matrix of diag(1, 1, −1, −1). It is therefore unnecessary to calibrate the Mueller matrices of the SM at different incidence angles, and moreover, the measured Mueller matrices are nothing but the Mueller matrices of the OL under test in double pass. Nevertheless, it is also noted that the reported setup in [21–23] is just for a conoscopic illumination mode where all incident light rays are converged at the focal point of the OL.

Inspired by the calibration setup in [21–23], we propose a versatile calibration method that can easily realize the calibration of polarization effect of a high-NA OL using MMP for not only the conoscopic illumination mode but also the orthoscopic illumination mode. In the latter case, the light rays are parallelly incident upon the sample and the incidence angles are scanned at the back focal plane of the OL. Since the Mueller matrix of any sample depends on both the polarization property of the sample *per se* and the illumination condition, such as wavelength and incidence angle, the Mueller matrices of a high-NA OL in the two illumination modes should be carefully calibrated for high-precision measurement. In the remainder of the paper, we firstly briefly introduce the basic working principle of MMP in section 2.1. Then, the calibration details in the conoscopic and orthoscopic illumination modes are presented in sections 2.2 and 2.3, respectively. In section 3, a high-NA OL with a NA of 0.95 is firstly exemplified to demonstrate the capability of the proposed calibration method using a house-developed dual rotating-compensator MMP, and then, experiments are performed on two standard SiO_2/Si thin film samples with thicknesses of 25 nm and 100 nm to verify the calibrated results. The polarization effect of a low-NA OL as well as the error induced by misalignment of the SM are discussed at the end of section 3. Finally, we draw some conclusions and show the outlook of the present calibration method in section 4.

2. Principle

2.1. Basic principle of MMP

The MMP is typically composed of a light source, a detector, a polarization state generator (PSG), and a polarization state analyzer (PSA). The PSG and PSA typically consist of identical polarization components such as polarizers (or analyzers) and compensators (also called retarders) but are arranged in a reverse order. The measurement of the sample Mueller matrix $\mathbf{M}$ involves a series of K ($K \geqslant 16$) flux measurements made by illuminating the sample with different polarization states and analyzing polarization states of the existing beam. The kth flux I_k measured by the detector is related to the sample Mueller matrix $\mathbf{M}$ by

$$I_k = \boldsymbol{A}_k^{\mathrm{T}} \mathbf{M} \boldsymbol{S}_k = (\boldsymbol{S}_k \otimes \boldsymbol{A}_k)^{\mathrm{T}} \boldsymbol{m}, \quad 1 \leqslant k \leqslant K, \tag{1}$$

where the symbol $\otimes$ denotes the Kronecker product, the superscript 'T' denotes the transpose, $\boldsymbol{S}_k = \mathbf{M}_{\mathrm{PSG}} \boldsymbol{S}_{\mathrm{in}}$ is the kth polarization state produced by the PSG with $\mathbf{M}_{\mathrm{PSG}}$ being the Mueller matrix of the PSG and $\boldsymbol{S}_{\mathrm{in}}$ being the Stokes vector of incident light from the light source and $\boldsymbol{S}_{\mathrm{in}} \propto [1,\ 0,\ 0,\ 0]^{\mathrm{T}}$, $\boldsymbol{A}_k = \mathbf{M}_{\mathrm{PSA}}^{\mathrm{T}} [1,\ 0,\ 0,\ 0]^{\mathrm{T}}$ is the kth existing polarization state produced by the PSA with $\mathbf{M}_{\mathrm{PSA}}$ being the Mueller matrix of the PSA, and $\boldsymbol{m}$ is the vectorization of the Mueller matrix $\mathbf{M}$, i.e. $\boldsymbol{m} = [M_{11},\ M_{21},\ M_{31},\ M_{41},\ M_{12},\ M_{22},\ \ldots,\ M_{34},\ M_{44}]^{\mathrm{T}}$. Writing equation (1) in a matrix form as

$$\boldsymbol{I} = \mathbf{D}\boldsymbol{m}, \tag{2}$$

where $\boldsymbol{I}$ is a $K \times 1$ column vector with the kth element being I_k, and the instrument matrix $\mathbf{D}$ is a $K \times 16$ matrix with the kth row vector being $(\boldsymbol{S}_k \otimes \boldsymbol{A}_k)^{\mathrm{T}}$. The instrument matrix $\mathbf{D}$ is a function of the instrumental system parameters that needs to be calibrated prior to the measurement, such as the transmission-axis orientation of the polarizer (analyzer) and the initial fast-axis orientation and phase retardance of the retarder (compensator). According to equation (2), the sample Mueller matrix can be measured by

$$\boldsymbol{m} = \mathbf{D}^{+} \boldsymbol{I}, \tag{3}$$

where $\mathbf{D}^{+} = (\mathbf{D}^{\mathrm{T}}\mathbf{D})^{-1}\mathbf{D}^{\mathrm{T}}$ is the Moore–Penrose pseudo-inverse of $\mathbf{D}$. Equations (1)–(3) present the basic and general principle of sample Mueller matrix measurement of any type of Mueller matrix polarimeters, such as the Mueller matrix polarimeters based on the dual rotating-compensator [24], the coupled ferroelectric liquid crystal cells [25], and the four photoelastic modulators [26].

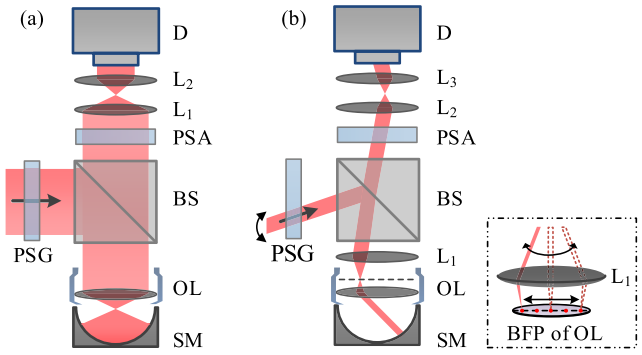

Figure 1. Configurations of calibration in (a) the conoscopic illumination mode and (b) the orthoscopic illumination mode. The inset on the right side of figure (b) presents the scanning on the back focal plane (BFP) of the OL to change the illumination directions. PSG, polarization state generator; PSA, polarization state analyzer; BS, beam splitter; OL, objective lens; SM, spherical mirror; L_1–L_3, lenses; D, detector.

2.2. Calibration in the conoscopic illumination mode

Figure 1(a) presents the calibration setup in the conoscopic illumination mode with MMP. Assume that the MMP here has been well calibrated. As can be seen from this figure, a collimated light beam passes successively through the PSG, a non-polarizing beam splitter (BS), and is converged by a high-NA OL. A SM is adopted as a reference sample, whose center is placed to coincide with the front focal point of the OL. In this case, each illuminating light ray is normally incident upon the SM and then reflects back along the same path. Afterwards, by means of two relay lenses, L_1 and L_2, each pixel of the detector represents a point on the back focal plane of the OL, which corresponds to a Mueller matrix in a polar coordinate. Note that the diameter of the collimated beam should be larger than that of the aperture of the OL so that the polarization effect of the whole back focal plane of the OL could be detected. In the calibration setup shown in figure 1(a), the finally measured Mueller matrix $\mathbf{M}_\mathrm{m}$ by the MMP should be expressed as the product of a series of Mueller matrices as follows

$$\mathbf{M}_\mathrm{m} = \mathbf{M}_\mathrm{t}^\mathrm{BS} \cdot \mathbf{M}_\mathrm{Cono}^\mathrm{OL} \cdot \mathbf{M}_\mathrm{SM} \cdot \mathbf{M}_\mathrm{Cono}^\mathrm{OL} \cdot \mathbf{M}_\mathrm{r}^\mathrm{BS}, \tag{4}$$

where $\mathbf{M}_\mathrm{r}^\mathrm{BS}$ and $\mathbf{M}_\mathrm{t}^\mathrm{BS}$ are the reflection and transmission Mueller matrices of the BS, respectively, which represent the residual polarization effect of the employed BS, $\mathbf{M}_\mathrm{SM}$ is the Mueller matrix of the SM and $\mathbf{M}_\mathrm{SM} = \mathrm{diag}(1,\ 1,\ -1,\ -1)$, which corresponds to the Mueller matrix for reflection at normal incidence [27], and $\mathbf{M}_\mathrm{Cono}^\mathrm{OL}$ denotes the Mueller matrix of the high-NA OL in the conoscopic illumination mode. Note that in equation (4) we assume the constituent materials of the OL are reciprocal. $\mathbf{M}_\mathrm{r}^\mathrm{BS}$ and $\mathbf{M}_\mathrm{t}^\mathrm{BS}$ can be determined by the MMP before inserting the lenses (OL, L_1, and L_2) into the calibration setup shown in figure 1(a). We can thereby obtain the Mueller matrix $\mathbf{M}_\mathrm{Cono}^\mathrm{OL}$ of the OL by

$$\mathbf{M}_\mathrm{Cono}^\mathrm{OL} = \left[(\mathbf{M}_\mathrm{t}^\mathrm{BS})^{-1} \cdot \mathbf{M}_\mathrm{m} \cdot (\mathbf{M}_\mathrm{r}^\mathrm{BS})^{-1} \cdot \mathbf{M}_\mathrm{SM}\right]^{1/2} \cdot (\mathbf{M}_\mathrm{SM})^{-1}. \tag{5}$$

2.3. Calibration in the orthoscopic illumination mode

Figure 1(b) presents the calibration setup in the orthoscopic illumination mode with MMP. Assume that the MMP here has also been well calibrated. Compared with figure 1(a), another lens L_1 (with a low NA) is introduced into the orthoscopic illumination mode to make the collimated light beam reflected by the BS parallelly illuminate on the SM with a certain illumination direction after the OL. Here, the center of the SM is also placed to coincide with the front focal point of the OL to guarantee that the illuminating light is normally incident upon the SM. Due to the small illuminating spot size (~100 μm), the reflection on the surface of the SM can be approximated to be a normal plane reflection. The Mueller matrices obtained from different pixels within the illuminating spot are approximated to be identical. In addition, as schematically shown in figure 1(b), the illumination direction of the light after the OL can be scanned from 0° to a maximum determined by the NA of the OL to calibrate the polarization effect of the OL at different illumination directions. For any illumination direction, the finally measured Mueller matrix $\mathbf{M}'_\mathrm{m}$ by the MMP can be expressed by

$$\mathbf{M}'_\mathrm{m} = \mathbf{M}_\mathrm{t}^\mathrm{BS} \cdot \mathbf{M}_\mathrm{Ortho}^\mathrm{OL} \cdot \mathbf{M}_\mathrm{SM} \cdot \mathbf{M}_\mathrm{Ortho}^\mathrm{OL} \cdot \mathbf{M}_\mathrm{r}^\mathrm{BS}, \tag{6}$$

where $\mathbf{M}_\mathrm{r}^\mathrm{BS}$ and $\mathbf{M}_\mathrm{t}^\mathrm{BS}$ are the reflection and transmission Mueller matrices of the BS, respectively, $\mathbf{M}_\mathrm{SM} = \mathrm{diag}(1,\ 1,\ -1,\ -1)$ is the Mueller matrix of the SM, and $\mathbf{M}_\mathrm{Ortho}^\mathrm{OL}$ denotes the Mueller matrix of the high-NA OL in the orthoscopic illumination mode. Note that in equation (6) we also assume the constituent materials of the OL are reciprocal. Moreover, the polarization effect of L_1 is ignored in the analysis due to its low NA (The rationality of the ignorable polarization effect of a low-NA lens will be discussed in section 3.3). Provided that $\mathbf{M}_\mathrm{r}^\mathrm{BS}$ and $\mathbf{M}_\mathrm{t}^\mathrm{BS}$ have been known, we can obtain $\mathbf{M}_\mathrm{Ortho}^\mathrm{OL}$ by

$$\mathbf{M}_\mathrm{Ortho}^\mathrm{OL} = \left[(\mathbf{M}_\mathrm{t}^\mathrm{BS})^{-1} \cdot \mathbf{M}'_\mathrm{m} \cdot (\mathbf{M}_\mathrm{r}^\mathrm{BS})^{-1} \cdot \mathbf{M}_\mathrm{SM}\right]^{1/2} \cdot (\mathbf{M}_\mathrm{SM})^{-1}. \tag{7}$$

As can be observed, the right sides of equations (5) and (7) look quite similar apart from the two Mueller matrices $\mathbf{M}_\mathrm{m}$ and $\mathbf{M}'_\mathrm{m}$ measured in different illumination modes. The Mueller matrices $\mathbf{M}_\mathrm{m}$ and $\mathbf{M}'_\mathrm{m}$ are generally different, since the Mueller matrix of any sample depends on not only the polarization property of the sample but also the illumination condition. In addition, it should be noted that the above calibration processes in the two illumination modes are both carried out in the global *x*-*y* coordinate system. A rotation matrix must be applied to the directly obtained Mueller matrices by equations (5)and (7) pixel-by-pixel to rotate them from the *x*-*y* coordinate system to the traditional *p*-*s* coordinate system used for the description of polarization by

$$\mathbf{M}_{\mathrm{Cono\ (Ortho)}}^\mathrm{OL}(p,\ s) = \mathbf{R}(-\varphi) \cdot \mathbf{M}_{\mathrm{Cono\ (Ortho)}}^\mathrm{OL}(x,\ y) \cdot \mathbf{R}(\varphi), \tag{8}$$

where $\mathbf{R}(\varphi)$ is the Mueller rotation transformation matrix for rotation by an angle φ. The definitions of the *x*-*y* coordinate system, the *p*-*s* coordinate system, and the angle φ are illustrated in figure 2. It is also noted from equations (5) and (7) that the calibration of the matrices $\mathbf{M}_\mathrm{Cono}^\mathrm{OL}$ and $\mathbf{M}_\mathrm{Ortho}^\mathrm{OL}$ involves

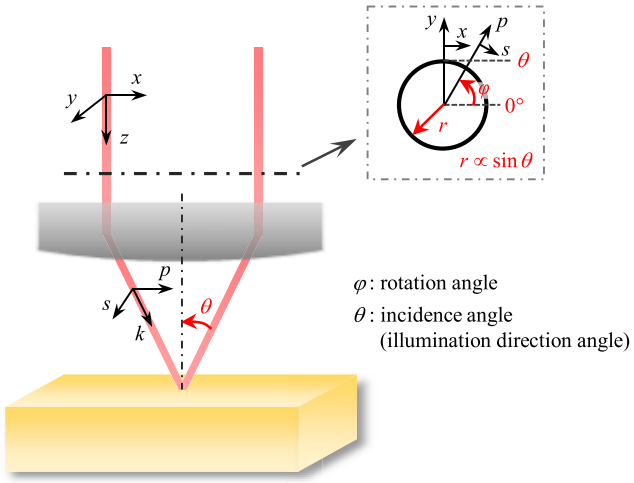

Figure 2. The relation between the global *x*-*y* coordinate system and the local *p*-*s* coordinate system. The inset shows the view against the *z*-direction. Note that here the angle θ is defined as the angle between the propagation direction of light beam and the optical axis, which is sometimes referred to as the illumination direction angle when there is no unique plane of incidence at normal incidence.

calculating the square root of a matrix, which will deliver several solutions in general. To choose the correct solution, we assume that the Mueller matrix of the high-NA OL should not deviate too much (For example, the Mueller matrix elements should not deviate from a positive value to a negative value, and vice versa.) from that of a general lens, whose Mueller matrix is approximately an identity matrix.

3. Results and discussion

3.1. Calibration results

To demonstrate the capability of the proposed calibration method, a well-calibrated dual rotating-compensator MMP [15] was adopted to calibrate the polarization effect of a strain-free OL with a high NA of 0.95 (Epiplan-Apochromat 50×/0.95, Carl Zeiss, Inc., German). It is noted from figure 1(b) that, in the orthoscopic illumination mode, an oblique beam (a maximal angle of inclination of about 7.5°) passes through the PSG and PSA of the MMP. To make the calibration credible, both the adopted polarizer (analyzer) and waveplates in the PSG and PSA have a large working acceptance angle (greater than 7.7°) that is enough for accurate measurement. All these polarization elements have also been tested by a commercial MME (ME-L, Wuhan Eoptics Technology Co., Ltd., China). The measurement results revealed that the corresponding Mueller matrices of these polarization elements were almost identical within the range of the acceptance angle. As for the BS, its reflection and transmission properties were measured by the commercial MME at different incident angles in advance, which were then substituted into equations (5) and (7) in the calibration. As an example, figure 3 presents the calibrated Mueller matrices of the investigated OL. Figures 3(a) and (b) present the calibration results in the conoscopic illumination mode at the illumination wavelengths of 633 nm and 488 nm, respectively. Figures 3(c) and (d) present the calibration results in the orthoscopic illumination mode at the illumination wavelengths of 633 nm and 488 nm, respectively. In both calibration modes, the maximum illumination direction angle was set to be 65° due to the restriction of the mechanical structure of the calibration system, although the maximum illumination direction could be up to 71.8° for an OL of NA = 0.95 in theory.

It is known that the two 2 × 2 off-diagonal blocks of the Mueller matrix of an isotropic sample vanish while other elements can be expressed in terms of conventional ellipsometric angles Ψ and Δ, i.e. $M_{12} = M_{21} = -\cos 2\Psi$, $M_{34} = -M_{43} = \sin 2\Psi \sin\Delta$, and $M_{33} = M_{44} = \sin 2\Psi \cos\Delta$ ($M_{11} = M_{22} = 1$). However, it should be noted that the nonzero 2 × 2 off-diagonal block elements of the calibrated Mueller matrices shown in figure 3 do not necessarily indicate that the OL under test are anisotropic, but are mainly induced by the measurement errors. As can be observed from figure 3, the Mueller matrices of the OL, especially their two 2 × 2 diagonal block elements, calibrated in both calibration modes and at both wavelengths exhibit similar axial symmetry and trend. Specifically, in the central part, the elements M_{33} and M_{44} are extremely close to 1, while the elements M_{12}, M_{21}, M_{34} and M_{43} are extremely close to 0. With the increase of the illumination direction angle, the elements M_{33} and M_{44} monotonically deviate from 1 and other elements M_{12}, M_{21}, M_{34} and M_{43} deviate from 0. Largest deviation is reached in the maximum illumination direction. It is noted that similar axial symmetry and trend in the Mueller matrices of a high-NA OL can also be observed from the reported literature [21–23].

Although 16 elements of a 4 × 4 Mueller matrix contain all the polarization information that one can extract from a linear polarization scattering process, it is usually difficult to directly obtain the polarization properties of a sample from the measured Mueller matrices. To this end, various Mueller matrix decomposition strategies [28] have been proposed over the past years, of which the Lu-Chipman polar decomposition [29] was adopted to extract the polarization properties hidden in the calibrated Mueller matrices shown in figure 3. According to the Lu-Chipman polar decomposition, any Mueller matrix $\mathbf{M}$ can be decomposed into a product of three Mueller matrices, that is, $\mathbf{M} = \mathbf{M}_\Delta \mathbf{M}_R \mathbf{M}_D$, where $\mathbf{M}_\Delta$, $\mathbf{M}_R$ and $\mathbf{M}_D$ correspond to the Mueller matrices of a depolarizer, a retarder and a diattenuator, respectively. The polarization properties, such as the retardance R, the diattenuation D, and the depolarization power Δ, can be further calculated from the decomposed Mueller matrices $\mathbf{M}_R$, $\mathbf{M}_D$, and $\mathbf{M}_\Delta$, respectively. Detailed equations to calculate the above polarization properties are omitted here for the sake of brevity. One can consult [29] for more details. The amplitude-ratio angle Ψ between the *p*- and *s*-polarizations could then be obtained by $\Psi = [\cos^{-1}(D)]/2$ ($0 \leqslant D \leqslant 1$ as defined in [29]). Figure 4 exemplifies the amplitude-ratio angle Ψ and retardance R of the OL under test extracted from the Mueller matrix shown in figure 3(a) calibrated in the conoscopic illumination mode at the wavelength of 633 nm. Since the extracted depolarization index from the calibrated Mueller matrix is rather small (less

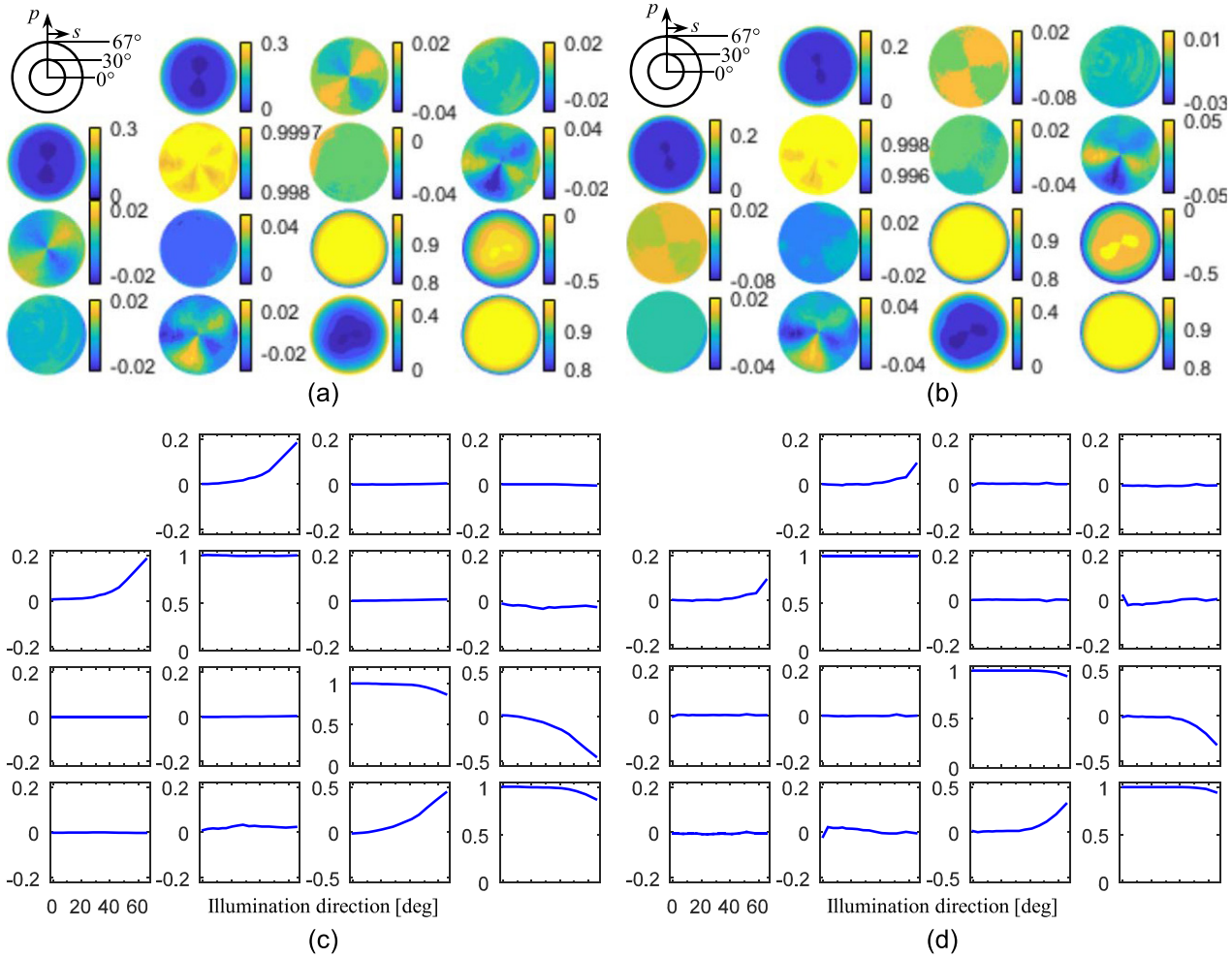

Figure 3. Calibrated Mueller matrices (normalized to M_{11}, which is not shown) of a high-NA OL (NA = 0.95). Measurement configurations were set as: (a) in the conoscopic illumination mode at the wavelength of 633 nm; (b) in the conoscopic illumination mode at the wavelength of 488 nm; (c) in the orthoscopic illumination mode at the wavelength of 633 nm; (d) in the orthoscopic illumination mode at the wavelength of 488 nm. The insets in (a) and (b) show the correspondence between the illumination direction and the radius of each circular panel, as schematically shown in figure 2.

than 1.8×10^{-3}), it was thereby not presented in figure 4. Similar axial symmetry and trend to those shown in figure 3 can be easily observed from figure 4. The results shown in figures 3 and 4 therefore indicate that the polarization effect of a high-NA OL is negligible in its central part but should be taken into account near its outmost margin.

3.2. Thin film testing

To verify the above calibration results, two standard SiO_2/Si thin film samples with nominal thicknesses of 25 nm and 100 nm were measured by MMP with the high-NA OL under test (namely the calibration setups shown in figure 1 by replacing the SM with the thin film samples). Experiments were performed at the wavelength of 633 nm and in the range of incidence angles from 50° to 63°. The analysis results obtained without considering the polarization effect of the high-NA OL were compared with those obtained by taking the polarization effect of the high-NA OL into account. In addition, the standard thin film samples were also measured by the commercial MME to provide a reference for the comparison.

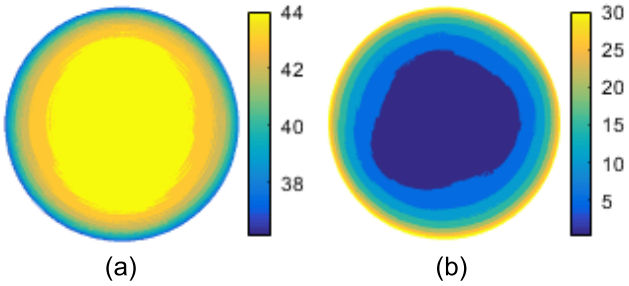

Figure 4. (a) The amplitude-ratio angle Ψ between the *p*- and *s*- polarizations and (b) the retardance *R* of the high-NA OL (NA = 0.95) extracted from the Mueller matrix shown in figure 3(a) calibrated in the conoscopic illumination mode at the wavelength of 633 nm. The units of the two legend bars are in degree.

Figures 5(a) and (b) present the comparison of Mueller matrices of the SiO_2/Si thin film samples measured by the commercial MME, the MMP with high-NA OL using the calibration results given in figure 3, and the MMP with high-NA OL without considering the polarization effect of the OL, respectively. Since the results measured by the above

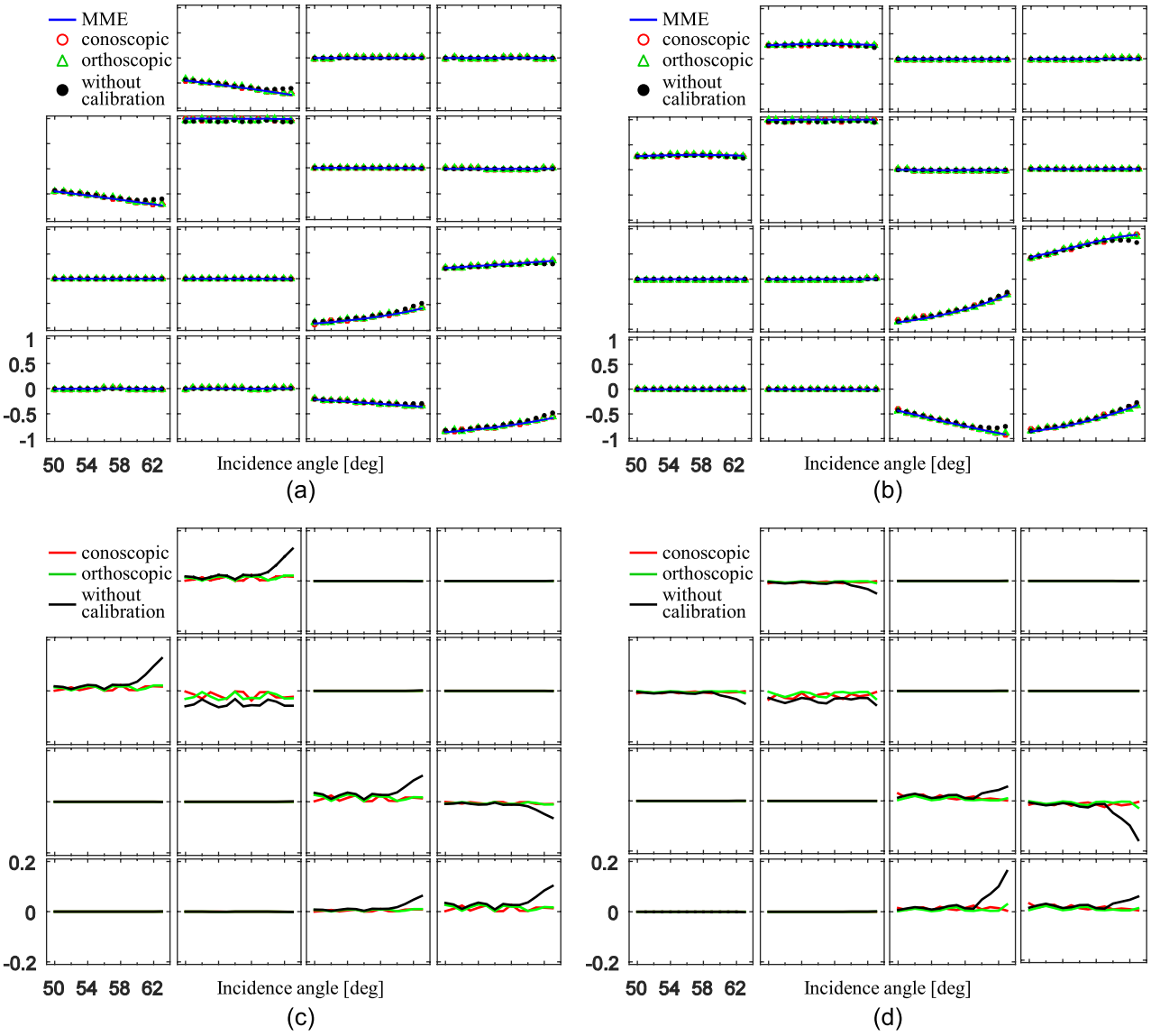

Figure 5. Comparison of the measured Mueller matrices (normalized to M_{11}) of the (a) 25 nm and (b) 110 nm SiO_2/Si thin film samples at the wavelength of 633 nm. The blue solid line, the red circle, the green triangle, and the black dot correspond to the results measured by the commercial MME, the MMP with high-NA OL using the calibration result in the conoscopic illumination mode, the MMP with high-NA OL using the calibration result in the orthoscopic illumination mode, and the MMP with high-NA OL without considering the polarization effect of the OL, respectively. Difference between the Mueller matrices measured by the MMP with high-NA OL and those by the commercial MME for the (c) 25 nm thin film sample and (d) 110 nm thin film sample. The red, green, and black solid lines correspond to the results measured by MMP with high-NA OL using the calibration result in the conoscopic illumination mode, using the calibration result in the orthoscopic illumination mode, and without considering the polarization effect of the OL, respectively.

different approaches are too close to each other, the difference with respect to the MME-measured results is presented in figures 5(c) and (d) to reveal the discrepancy between the results measured by MMP with high-NA OL before and after calibration of the polarization effect of the OL. As can be observed from figures 5(c) and (d), the discrepancy induced by the polarization effect of the OL is ignorable in smaller incidence angles (less than 60°); however, the discrepancy becomes more and more striking in larger incidence angles (larger than 60°, closer to the outmost margin of the OL), which is in accordance with the previous prediction drawn from figures 3 and 4. More importantly, after calibration, the Mueller matrices measured by MMP with high-NA OL are in good accordance with those measured by MME. Table 1 further presents the discrepancy between the extracted film thicknesses from the Mueller matrices measured by MMP with high-NA OL before and after calibration the polarization effect of the OL. Although the discrepancy is not very large, as confirmed by the measurement results by the commercial MME, the results shown in figure 5 and table 1 definitely verify the necessity in calibration of the polarization effect of high-NA OL as well as the feasibility of the proposed calibration method.

It is revealed from figure 5 that the Mueller matrix $\mathbf{M}^{\mathrm{OL}}_{\mathrm{Ortho}}$ calibrated in the orthoscopic illumination mode does not show a noticeable difference to that $\mathbf{M}^{\mathrm{OL}}_{\mathrm{Cono}}$ calibrated in the conoscopic illumination mode, although $\mathbf{M}^{\mathrm{OL}}_{\mathrm{Cono}}$ and $\mathbf{M}^{\mathrm{OL}}_{\mathrm{Ortho}}$ should be different according to equations (5) and (7). The main reason may be the finite spot size of light beam incident upon

Table 1. Comparison of measured film thicknesses of the standard SiO_2/Si thin film samples.

Sample	Without calibration (nm)	Calibration in conoscopic illumination mode (nm)	Calibration in orthoscopic illumination mode (nm)	Commercial MME (nm)
25 nm	24.5	24.1	24.1	23.4
110 nm	114.1	113.2	113.2	112.1

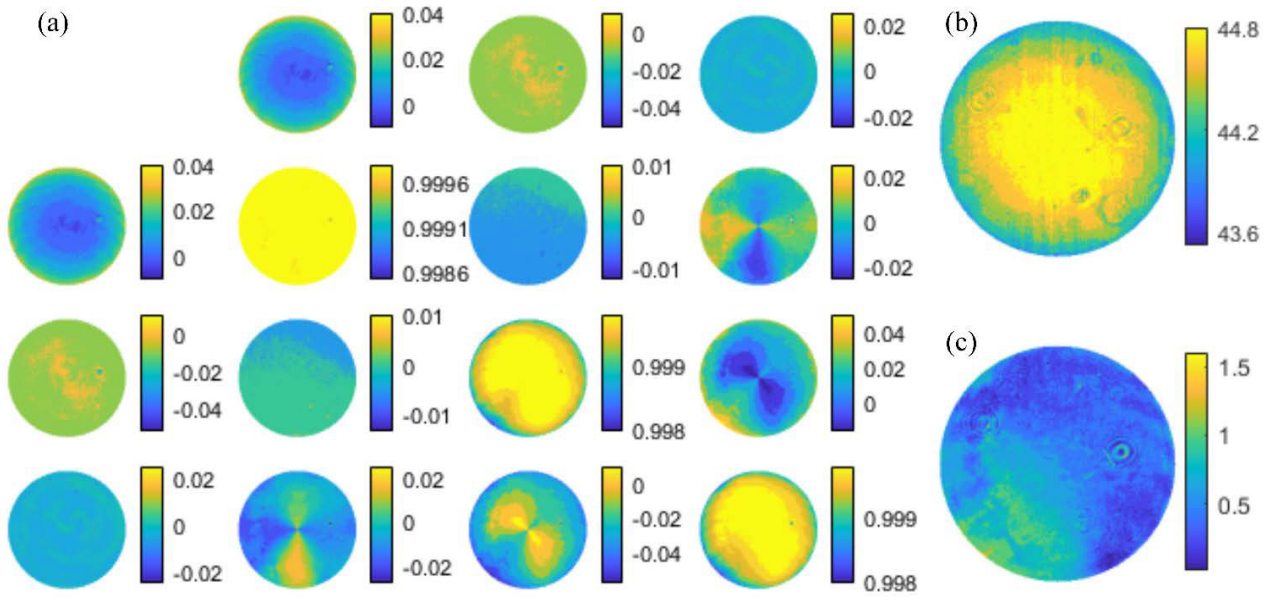

Figure 6. (a) Calibrated Mueller matrix (normalized to M_{11}) of a low-NA OL (NA = 0.55) in the conoscopic illumination mode at the wavelength of 633 nm; the (b) diattenuation and (c) retardance of the low-NA OL extracted from the calibrated Mueller matrix. The units of the legend bars of (b) and (c) are in degree.

the BFP of the OL and the surface of the SM in the orthoscopic illumination mode. It is hard for us to estimate the spot size on the BFP of the OL, while the spot size on the surface of the SM is about 100 μm, which leads to the reflected beam spreading out as it propagates back to the OL. In addition, as can be observed from the 2 × 2 off-diagonal block elements of the calibrated Mueller matrices in figures 3(a) and (b), the measurement errors of the instrument may hide the difference between $\mathbf{M}^{\mathrm{OL}}_{\mathrm{Cono}}$ and $\mathbf{M}^{\mathrm{OL}}_{\mathrm{Ortho}}$.

3.3. Discussion

3.3.1. Polarization effect of a low-NA OL. It is known from sections 3.1 and 3.2 that the polarization effect of a high-NA OL cannot be ignored. We want to further examine the polarization effect of a low-NA OL, since we have assumed in section 2.3 that the polarization effect of the low-NA lens, L_1 in figure 1(b), is ignored in analysis. A strain-free OL with a low NA of 0.55 (M Plan Apo 50×/0.55, Mitutoyo, Inc., Japan) was measured in the conoscopic calibration mode at the wavelength of 633 nm. Figure 6 presents the calibrated Mueller matrix as well as the decomposed diattenuation and retardance of the low-NA OL under test. As can be observed from figure 6, the Mueller matrix of the OL approaches to a unit matrix while the associated diattenuation and retardance approach to 45° and 0°, respectively, over the whole focal plane of the OL (small deviation is induced by measurement errors). Clearly, the polarization effect of a low-NA OL can be ignored in practice.

3.3.2. Error analysis due to misalignment of the spherical mirror. The basic idea in the proposed calibration method is to use the special form of the Mueller matrix of a sample at normal reflection, namely diag(1, 1, −1, −1). A key in the implementation of the calibration method is therefore to accurately align the center of the spherical mirror, SM, to make it in coincidence with the front focal point of the OL under test to guarantee that the illuminating light is normally incident upon the SM. A misalignment of the SM will lead the Mueller matrix of the SM deviate from the ideal diagonal matrix to the general form corresponding to an isotropic sample. Take the conoscopic calibration mode as an example, equation (4) in this case should be rewritten as

$$\mathbf{M}_{\mathrm{m}} = \mathbf{M}^{\mathrm{BS}}_{\mathrm{t}} \cdot \mathbf{M}^{\mathrm{OL}'}_{\mathrm{Cono2}} \cdot (\mathbf{M}_{\mathrm{SM}} + \Delta\mathbf{M}_{\mathrm{SM}}) \cdot \mathbf{M}^{\mathrm{OL}'}_{\mathrm{Cono1}} \cdot \mathbf{M}^{\mathrm{BS}}_{\mathrm{r}}, \tag{9}$$

where $\mathbf{M}_{\mathrm{SM}} = \mathrm{diag}(1,\ 1,\ -1,\ -1)$ and $\Delta\mathbf{M}_{\mathrm{SM}}$ represents the deviation error resulted in misalignment of the SM. Since the incident and reflected light may pass through different locations of the back focal plane of the OL at oblique incidence, the Mueller matrix of the OL in the incident and reflected paths is generally denoted as $\mathbf{M}^{\mathrm{OL}'}_{\mathrm{Cono1}}$ and $\mathrm{M}^{\mathrm{OL}'}_{\mathrm{Cono2}}$ in equation (9), respectively.

Simulation was performed in the conoscopic calibration mode to evaluate the error in the calibrated Mueller matrix of

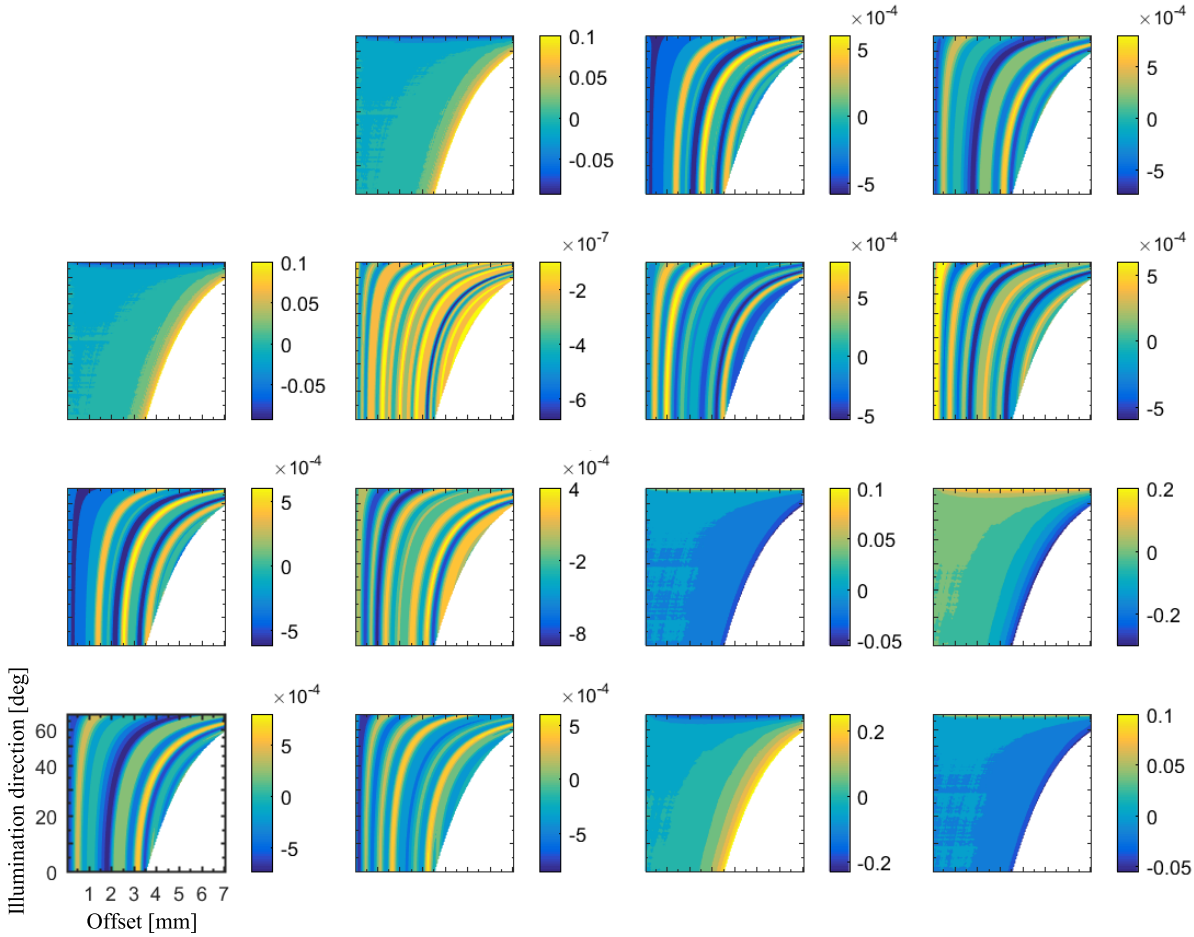

Figure 7. Estimated error $\Delta\mathbf{M}_{\mathrm{Cono}}^{\mathrm{OL}}$ in the calibrated Mueller matrix of the high-NA OL (NA = 0.95) induced by misalignment of the SM. The abscissa axis represents the offset (0–7 mm) between the center of the SM and the front focal point of the OL, and the ordinate axis represents the illumination direction (0–67°) as shown in the inset.

the OL due to misalignment of the SM. In the simulation, we first synthesized the Mueller matrix of a high-NA OL, $\mathbf{M}_{\mathrm{Cono}}^{\mathrm{OL}}$, using the calibrated data given in figure 4. We then calculated $\Delta\mathbf{M}_{\mathrm{SM}}$ at different misalignments of the center of the SM with respect to the front focal point of the OL. In the calculation, the SM was modeled as a SiO_2 film layer on an Ag film layer deposited on a fused Si substrate. The thickness of the SiO_2 film was 1 μm and the Ag film layer was thick enough to prevent light penetrating through it. Due to the rotational symmetry of the OL, it was enough to calculate $\Delta\mathbf{M}_{\mathrm{SM}}$ along any axial direction. The $\mathbf{M}_{\mathrm{Cono1}}^{\mathrm{OL}'}$ and $\mathbf{M}_{\mathrm{Cono2}}^{\mathrm{OL}'}$ in equation (9) were obtained by interpolating the synthesized Mueller matrix $\mathbf{M}_{\mathrm{Cono}}^{\mathrm{OL}}$ according to the specific oblique angle estimated by the corresponding misalignment. With the calculated ΔM_{SM} as well as $\mathbf{M}_{\mathrm{Cono1}}^{\mathrm{OL}'}$ and $\mathbf{M}_{\mathrm{Cono2}}^{\mathrm{OL}'}$, we could simulate the measured Mueller matrix $\mathbf{M}_{\mathrm{m}}$ by equation(9). Finally, we calculated the Mueller matrix of the OL, $\mathbf{M}_{\mathrm{Cono}}^{\mathrm{OL}'}$, by equation (5) and estimated the error $\Delta\mathbf{M}_{\mathrm{Cono}}^{\mathrm{OL}} = \mathbf{M}_{\mathrm{Cono}}^{\mathrm{OL}} - \mathbf{M}_{\mathrm{Cono}}^{\mathrm{OL}'}$, which would be error in the calibrated Mueller matrix of OL induced by misalignment of the SM.

Figure 7 presents the estimated error $\Delta\mathbf{M}_{\mathrm{Cono}}^{\mathrm{OL}}$ in the calibrated Mueller matrix of the high-NA OL at different offsets of the SM and different illumination directions. The blank part shown at the bottom-right side of each panel corresponds to the situation where the reflected light by the SM could not be collected by the OL any more when the offset is greater than 3.5 mm. As can be observed from figure 7, the 2 × 2 off-diagonal block elements are always rather small, since the misalignment of the SM leads the Mueller matrix of the SM to be the general form corresponding to an isotropic sample, which primarily affects the 2 × 2 diagonal block elements (except M_{22}). As expected, the errors in the 2 × 2 diagonal block elements become more noticeable at larger offsets and larger illumination direction angles. Moreover, at large illumination direction angles (larger than 63°), even a minor offset of 0.5 mm will lead to a large error of about 0.2 in the elements M_{34} and M_{43}. It therefore suggests that the offset between the center of the SM and the front focal point of the OL should be less than 0.5 mm in the calibration of the OL. The alignment error can be minimized using an interferometric technique as reported in [23].

4. Conclusions

A calibration method about the polarization effect of an OL using MMP has been proposed in this work. Two calibration setups have been presented in detail to show the calibration

in the conoscopic and orthoscopic illumination modes, respectively. Two OLs, one with NA = 0.95 and another with NA = 0.55, were exemplified to demonstrate the capability of the proposed calibration method using a house-developed dual rotating-compensator MMP. The experimental results have revealed that the polarization effects of the high-NA OL near its central part and the low-NA OL were ignorable; however, the polarization effect of the high-NA OL near its outmost margin should be taken into account in practice. The error induced by the misalignment of a key component, the spherical mirror, in the proposed calibration method was finally discussed. Compared with the existing calibration methods, the proposed method is much simpler and more efficient for implementation, and more importantly, the calibrated data, 16 elements of a 4×4 Mueller matrix, contains all the polarization information that one can extract from a linear polarization scattering process. It is therefore expected that the proposed calibration method could provide a more complete polarization characterization of the high-NA OL and would gain wider applications in calibrating the polarization effect of the high-NA OL.

Acknowledgments

This work was funded by the National Natural Science Foundation of China (Grant Nos. 51775217, 51727809, 51475191, and 51525502), the National Science and Technology Major Project of China (Grant No. 2017ZX02101006-004), and the National Science Foundation of Hubei Province of China (Grant Nos. 2018CFB559 and 2018CFA057).

ORCID iDs

Xiuguo Chen https://orcid.org/0000-0002-7067-5084
Hao Jiang https://orcid.org/0000-0003-0561-5058
Shiyuan Liu https://orcid.org/0000-0002-0756-1439

References

[1] Nesse W 2012 *Introduction to Optical Mineralogy* 4th edn (New York: Oxford University Press)
[2] Wood E A 1977 *Crystals and Light: Introduction to Optical Crystallography* (New York: Dover)
[3] Inoué S and Sato H 1962 Arrangement of DNA in living sperm: a biophysical analysis *Science* **136** 1122–4
[4] Vrabioiu A M and Mitchison T J 2006 Structural insights into yeast septin organization from polarized fluorescence microscopy *Nature* **443** 466–49
[5] Wang Y, He H, Chang J, He C, Liu S, Li M, Zeng N, Wu J and Hui Ma 2016 Mueller matrix microscope: a quantitative tool to facilitate detections and fibrosis scorings of liver cirrhosis and cancer tissues *J. Biomed. Opt.* **21** 071112
[6] Serrels K A, Ramsay E, Warburton R J and Reid D T 2008 Nanoscale optical microscopy in the vectorial focusing regime *Nat. Photon.* **2** 311–4
[7] Zhang T, Ruan Y, Maire G, Sentenac D, Talneau A, Belkebir K, Chaunet P C and Sentenac A 2013 Full-polarized tomographic diffraction microscopy achieves a resolution about one-fourth of the wavelength *Phys. Rev. Lett.* **111** 243904
[8] Fallet C, Novikova T, Foldyna M, Manhas S, Ibrahim B H, De Martino A, Vannuffel C and Constancias C 2011 Overlay measurements by Mueller polarimetry in back focal plane *J. Micro/Nanolith. MEMS MOEMS* **10** 033017
[9] Tan Y, Chen C, Chen X, Du W, Gu H and Liu S 2018 Development of a tomographic Mueller-matrix scatterometer for nanostructure metrology *Rev. Sci. Instrum.* **89** 073702
[10] Chipman R A 1989 Polarization analysis of optical systems *Opt. Eng.* **28** 280290
[11] Shribak M, Inoué S and Oldenbourg R 2002 Polarization aberrations caused by differential transmission and phase shift in high NA lenses: theory, measurement and rectification *Opt. Eng.* **41** 943–54
[12] Totzeck M, Gräupner P, Heil T, Göhnermeier A, Dittmann O, Krähmer D, Kamenov V, Ruoff J and Flagello D G 2005 Polarization influence on imaging *J. Microlith. Microfab. Microsyst.* **4** 031108
[13] McIntyre G R, Kye J, Levinson H and Neureuther A R 2006 Polarization aberrations in hyper-numerical-aperture projection printing: a comparison of various representations *J. Microlith. Microfab. Microsyst.* **5** 033001
[14] Chipmann R A 2010 *Polarimetry Handbook of Optics* 3rd edn (New York: McGraw-Hill)
[15] Liu S, Chen X and Zhang C 2015 Development of a broadband Mueller matrix ellipsometer as a powerful tool for nanostructure metrology *Thin Solid Films* **584** 176–85
[16] McIntyre G R and Neureuther A R 2005 Phase-shifting mask polarimetry: monitoring polarization at 193-nm high numerical aperture and immersion lithography with phase shifting masks *J. Microlith. Microfab. Microsyst.* **4** 031102
[17] Li S, Wang X, Yang J, Duan L, Tang F and Yan G 2015 In situ aberration measurement method using a phase-shift ring mask *J. Micro/Nanolith. MEMS MOEMS* **14** 011005
[18] Shiode Y and Ebiahara T 2006 Study of polarization aberration measurement using SPIN method *Proc. SPIE* **6154** 615431
[19] Nomura H and Higashikawa I 2009 Mueller matrix polarimetry for immersion lithography tools with a polarization monitoring system at the wafer plane *Proc. SPIE* **7520** 752012
[20] Nomura H and Higashikawa I 2010 *In situ* Mueller matrix polarimetry of projection lenses for 193-nm lithography *Proc. SPIE* **7640** 76400Q
[21] Ibrahim B H, Hatit S B and De Martino A 2009 Angle resolved Mueller polarimetry with a high numerical aperture and characterization of transparent biaxial samples *Appl. Opt.* **48** 5025–34
[22] Rodríguez-Herrera O G, Lara D and Dainty C 2010 Far-field polarization-based sensitivity to sub-resolution displacements of a sub-resolution scatterer in tightly focused fields *Opt. Express* **18** 5609–28
[23] Rodríguez-Herrera O G 2009 Far-field method for the characterisation of three-dimensional fields: vectorial polarimetry *PhD Thesis* National University of Ireland
[24] Azzam R M A 1978 Photopolarimeter measurement of the Mueller matrix by Fourier analysis of a single detected signal *Opt. Lett.* **2** 148–50
[25] Garcia-Caurel E, Martino A and De adn Drévillon B 2004 Spectroscopic Mueller polarimeter based on liquid crystal devices *Thin Solid Films* **455–6** 120–3
[26] Arteaga O, Freudenthal J, Wang B and Kahr B 2012 Mueller matrix polarimetry with four photoelastic modulators: theory and calibration *Appl. Opt.* **51** 6805–17
[27] Goldstein D H 2011 *Polarized Light* 3rd edn (Boca Raton, FL: CRC Press)
[28] Gil J J and Ossikovski R 2016 *Polarized Light and the Mueller Matrix Approach* (Boca Raton, FL: CRC Press)
[29] Lu S Y and Chipman R A 1996 Interpretation of Mueller matrices based on polar decomposition *J. Opt. Soc. Am.* A **13** 1106–13